INTERNATIONAL ASSOCIATION OF BIOLOGICALS AND COMPUTATIONAL DIGEST
International & Peer-Reviewed Journal
E-ISSN: 2583-3995

EXPLORING THE ANTI-CANCER POTENTIAL OF PHYTOCHEMICALS FROM SPECIFIC PLANTS: EXAMINING AND VALIDATING THROUGH MOLECULAR DOCKING AND MD SIMULATIONS

Poojaben Prajapati[1], Bharat B. Maitreya[1], Rakesh M. Rawal[2]

[1]Department of Botany, Bioinformatics and Climate Change Impacts Management, School of Science, poojaprajapati@gujaratuniveristy.ac.in

[2]Department of Life Science, School of Science
Gujarat University, Ahmedabad, Gujarat, India-380009.
rakeshrawal@gujaratuniversity.ac.in

Corresponding author Email: bbmaitreya@gujaratuniversity.ac.in

NAME	ORCID
Poojaben Prajapati	0000-0002-6852-4260
Bharat Maitreya	0000-0001-6689-4543
Rakesh Rawal	0000-0002-7985-1187

ABSTRACT

Worldwide, cancer is the leading cause of death. Anti-cancer medications frequently induce side effects and multidrug resistance (MDR), which continues to be a key obstacle to effective cancer therapy. Essential nutrients and functionally bioactive substances can both be found in abundance in plants. The phytochemical components have great promise for treating both plant and human ailments. This study is designed to conduct an in-silico analysis on phytochemicals derived from Combretaceae family plants for targeting the proteins 4UWH, 5LWM, and 6P3D. The Combretaceae family has demonstrated pharmacological benefits such as anti-leishmanial, cytotoxic, antibacterial, antidiabetic, antiprotozoal, anticancer, and antifungal qualities. To conduct experiments with the natural phytochemicals against the proteins, computerized tools, online servers, and online databases were used. 196 natural compounds were used for virtual screening out of the top 5 best-docked compounds selected based on their binding energy. The best-selected phytochemicals possessed potential results in 10ns molecular dynamic simulation. So, it is convincible based on in-silico research this selected phytochemical has the potential to serve as a promising lead compound against cancer.

Keyword: *Combretaceae family plants, Phytochemicals, Molecular docking, Molecular Dynamic Simulation*

INTRODUCTION

As a tumour that is cancerous grows through the lymphatic or circulatory systems, cancer cells may spread to other parts of the body. During this phase, cancer cells grow and may develop new tumours. Cancer conceptualization is distinguished by a heuristic effort to condense the immense complexity of cancer phenotypes and genotypes into a preliminary set of guiding principles. Other areas of the disease have emerged as possible advancements as our understanding of cancer pathways has grown (Hanahan, 2022). There are over a hundred different types of cancer. The organs or tissues where tumours form are commonly utilised to identify the many forms of cancer (Ai *et al.*, 2021). Cancers can also be categorized based on the type of cell that caused them, such as epithelial or squamous cells. Cancer is the world's top cause of death and the second largest cause of death in the United States (Trayes and Cokenakes, 2021). Because of healthcare setting closures, changes in employment and health insurance, and fear of COVID-19 exposure, the coronavirus illness 2019 (COVID-19) pandemic caused cancer detection and treatment delays (Anderson *et al.*, 2021). Although the impact was greatest during the COVID-19 peak in mid2020, healthcare provision has not

fully recovered. For example, surgical oncology procedures at Massachusetts General Hospital were 72% of 2019 levels in the final half of 2020 and only 84% in 2021, the lowest recovery of any surgical specialty (Ghoshal *et al.*, 2022).

The Combretaceae, popularly known as the white mangrove family. Members of the family are found throughout the world's tropical and subtropical climates. The majority of the trees, shrubs, and lianas in the Combretaceae family are used medicinally (Eloff, Katerere and McGaw, 2008). Members of this family contain a variety of phytoconstituents with therapeutic potential, including as tannins, flavonoids, terpenoids, and alkaloids.

Figure1: Combretaceae family plant (Source:https://upload.wikimedia.org/wikipedia/commons/e/ec/Combretum_constrictum3.jpg)

Scientific classification

Kingdom: Plantae
Division: Angiospermae
Class: Dicotyledons
Subclass: Polypetalae
Order: Myrtales
Family: Combretaceae – Indian Almond family

Phytochemicals are naturally occurring, physiologically active chemical substances found in plants. They provide additional health benefits to humans that are not supplied by macronutrients and micronutrients (Factor, 2022). Phytochemical comes from the Greek term phyto, which meaning "plant." They not only improve the plant's colour, flavour, and scent, but they also protect it from injury and illness. Phytochemicals are plant molecules that protect plant cells from environmental threats like pollution, stress, dehydration, UV exposure, and pathogenic assault (Velavan, 2016).

Phosphoinositide 3-kinases (PI3Ks) are a type of lipid kinase that initiates intracellular signalling cascades that regulate a number of cellular processes. PI3K phosphorylates the 30 -OH group on phosphatidylinositols in the plasma membrane. As a result, AKT, a protein Ser/Thr kinase, is attracted to the cell membrane and activated there (Wong, Engelman and Cantley, 2010). The PI3K/AKT signalling cascade is critical in cancer because it promotes cell proliferation and survival. In cancer, multiple techniques are employed to activate PI3K-AKT signalling. Somatic mutations in the PIK3CA gene, which codes for the p110a catalytic subunit, have been detected in a number of solid tumours. The helical domain (E545K and E542K) and the kinase domain (H1047R) are the two most common locations for these alterations (Courtney, Corcoran and Engelman, 2010). JAK3 is essential for T-cell proliferation and immune system homeostasis because it is produced specifically in lymphoid cells and sends signals via the domain shared by the IL-2, IL-4, IL-7, IL-9, and IL-15 receptors (Hu *et al.*, 2021). Mutant JAK3 mutations were discovered in a small percentage of acute megakaryoblastic leukaemia patients, a high-risk childhood ALL case, and patients with cutaneous T-cell lymphoma (Kim *et al.*, 2020). BRAF encodes a protein kinase in the mitogen-activated protein kinase (MAPK) pathway that can be turned constitutively active by altering valine 600 (V600), most commonly to glutamic acid (V600E) (Hong *et al.*, 2012). Patients with BRAF-mutated mCRC are more likely to be female, older, and to have right-sided initial tumours (Fanelli *et al.*, 2020). They also have an unusual pattern of metastatic spread,

typically including peritoneal and distant lymph nodes. Serrated adenomas most typically characterise the BRAF mutation, which constitutes a separate molecular subtype of CRC, with high rates of hypermethylation and microsatellite instability (MSI) and low rates of chromosomal instability (Corcoran *et al.*, 2015).

Several computational tools for drug design have been developed during the last three decades, with promising results in drug identification (Keute *et al.*, 2019). Small molecules or ligands are sorted in molecular docking based on their optimum orientation on the target. The method may anticipate different ligand binding mechanisms in a target molecule's groove (Prajapati *et al.*, 2023). Quantum mechanics (ab initio and density functional theories) and molecular mechanics (docking, molecular dynamics, and protein folding) are two of these computational techniques. Docking and molecular dynamics are the most often used computational techniques for discovering cancer targets (Massarotti *et al.*, 2012). The technique of molecular docking is used to investigate the molecular behaviour of target proteins when they bind. It is a widely used instrument in pharmaceutical development. Yasara, AutoDock, Vina, Schrodinger, and GOLD are the top five software businesses, while AutoDock, Vina, MOE-Dock, FLexX, and GOLD are the most popular (Pinzi and Rastelli, 2019).

Table 1: List of Selected Combretaceae family plants

No.	Scientific name	Commonname	Activity
1	*Anogeissus acuminata*	Dhaura	Anticancer
2	*Combretum quadrangulare*	Sakae Naa	Anticancer
3	*Terminalia chebula*	black- or chebulic myrobalan	Anticancer
4	*Terminalia bellarica*	baheda	Anticancer
5	*Terminalia catappa L*	Indian almond	Anticancer
6	*Anogeissus latifolia*	Axlewood	Anticancer
7	*Combretum imberbe*	Leadwood Tree	Anticancer
8	*Guiera senegalensis*	Moshi medicine	Anticancer
9	*Combretum albidum*	Piluki	Anticancer
10	*Combretum indicum*	The Rangooncreeper	Anticancer
11	*Terminalia pallida*	Tropical almond	Anticancer
12	*Terminalia ivorensis*	Black Afara	Anticancer
13	*Lumnitzera racemosa*	White Teruntum	Anticancer
14	*Conocarpus erectus*	Silver Buttonwood	Anticancer
15	*Getonia floribunda*	Ukshi	Anticancer
16	*Terminalia alata*	Indian laurel	Anticancer

MATERIALS AND METHODS

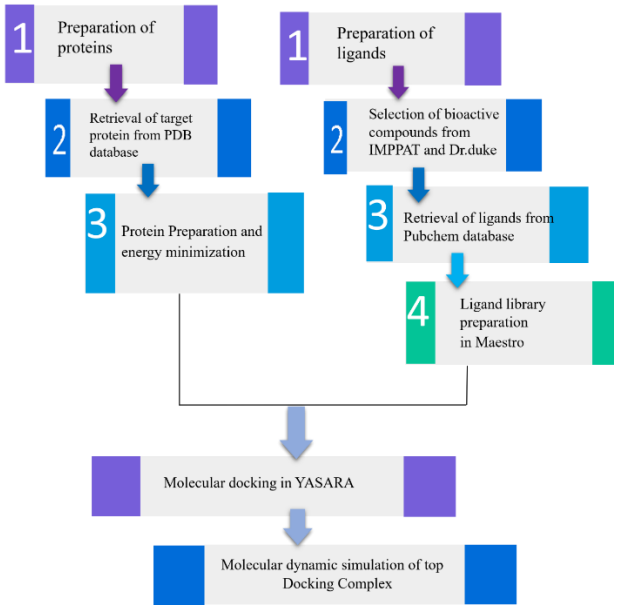

Figure 2: Graphical representation

Tools and database used

Protein selection and molecular docking were carried out using a variety of databases. After reading and analysing multiple articles, researchers uncovered more than three transcription factors involved in the cancer process. Based on the review of literature, 196 natural compounds were chosen for use in the PubChem database. The YASARA technology was used to investigate protein-DNA docking. These protein structures were obtained from the PDB database, cleaned, and water-added using the Discovery studio visualizer, and then Molecular Docking was performed using YASARA Software.

Protein preparation

PDB was used to obtain the three-dimensional protein structures. The first stage in protein preparation was to identify the specific transcription factors. This procedure cleansed the target protein while conserving energy. The YASARA software was used to generate the protein-ligand docking. The active site was discovered via the Discovery Studio visualizer, and the Simulation cell was constructed using the binding pocket in the active site.

Ligand Preparation

Phytochemicals retrieved from the Combretaceae family plant. Drawing, editing, and cleaning ligand structures using BIOVIA discovery studio visualizer. Then, the structure is converted into 2D and 3D formats and checked for errors. Moreover, it also included creating a single .sdf file for all 196 ligands in the Marvin sketch to facilitate docking.

Molecular Docking

Molecular docking is an important stage in virtual screening that is used to discover potential hits based on the interaction between the receptor and the ligand. The development of structure-based drugs is dependent on molecular docking. YASARA was used to acquire docking data for the listed chemicals with the corresponding target proteins. In this study, energy-efficient molecules were imported, docking conformations were performed twice using an evolutionary genetic approach, and the fitness of the docked structures was evaluated. The hydrogen bonds, residues, dissociation constants, and binding energies were estimated using the YASARA programme. As a starting point, the YASARA structure is used in protein binding pockets and ligand docking. Using its binding energy and a protein-ligand interaction analysis for several receptor proteins with the highest binding energy, the optimal binding ligand was discovered. Furthermore, the best-bound ligand's protein-ligand interaction is compared to that of its inbound ligand. YASARA was used for molecular docking studies. Molecular docking study was carried out using an Amber force field, which included water removal, chain selection, and energy minimization factors. We analyzed dock poses, docking energies, and interacting amino acid residues for predicting binding affinity using the following equation:

$\Delta G = \Delta GvdW + \Delta GHbond + \Delta Gelec + \Delta Gtor + \Delta Gdesolv$

Where,

$\Delta GvdW$ = Docking energy is referred to as van der Waals energy.

$\Delta GHbond$ = for docking energy, the H bonding term is used.

$\Delta Gelec$ = Docking energy is referred to as electrostatic energy.

$\Delta Gtor$ = When a ligand transitions from an unbound to a bound state, it has a torsional free energy term.

$\Delta Gdesolv$ = docking energy desolvation phrase (Patel *et al.*, 2021).

Molecular Dynamic Simulation

Using the YASARA Structure, the complex identified as a possible AChEIs was subjected to MD simulations. In the virtual screening, the best pose of the hit was chosen and afterwards prepared in a scene mode in YASARA Structure using the default mode. The scene mode was then subjected to MD simulations using the default settings of the YASARA Structure macro for MD run (http://www.yasara.org/md_run.mcr) (Krieger and Vriend, 2015), except for the MD length and snapshot intervals]. The MD run in this study lasted 10 ns, and the pictures were taken at 10 ps intervals (Liu, Watanabe and Kokubo, 2017). The production runs were analysed in the last 5 ns of the simulations, and the equilibrium states were regarded reached if the average deviation of the backbone atoms' root-mean-squared distances (RMSD) value was less than 1 (Liu, Watanabe and Kokubo, 2017). The free energy of binding (G) of each

snapshot of the enzyme-ligand binding in the final 5 ns of the MD simulations was also determined using VINA (Allouche, 2012)local search in the YASARA structure after the enzyme and peptide atoms were fixed (Krieger and Vriend, 2015).

RESULTS

Table 2: Top 5 Docking results of the protein PI3K (4UWH) docked with ligands.

Target protein	Compound name	Compound id	Bind .ener gy [kcal /mol]	Dissoc. constant [pM]	Contacting receptor residues
4UWH	Calycopterone	3036841	9.527 0	103900.2 031	A THR 610 A LEU 611 A PHE 612 A LYS 613 A SER 614 A PRO 618 A GLN 620 A ILE 634 A LYS 636 A TYR 670 A MET 682 A GLN 683 A PHE 684 A ILE 685 A SER 687 A VAL 688 A PRO 689 A GLU 692 A ASP 747 A LEU 750 A ILE 760
	Proanthocyanidin	108065	9.492 0	110222.8 750	A PHE 612 A LYS 613 A SER 614 A LEU 616 A PRO 618 A GLN 620 A ILE 634 A LYS 636 A TYR 670 A MET 682 A GLN 683 A PHE 684 A ILE 685 A SER 687 A PRO 689 A GLU 692 A ASP 747 A LEU 750 A PHE 758 A ILE 760
	1,3,6-Tri-O-galloyl-b-D-glucose	452707	9.462 0	115947.6 719	A ARG 566 A THR 610 A LEU 611 A PHE 612 A LYS 613 A SER 614 A LEU 616 A GLN 620 A ILE 634 A LYS 636 A TYR 670 A MET 682 A GLN 683 A PHE 684 A ILE 685 A SER 687 A PRO 689 A ASP 747 A LEU 750 A PHE 758 A ILE 760 A ASP 761

	celastrol	122724	9.1120	209322.2656	A PHE 612 A LYS 613 A SER 614 A PRO 618 A ILE 634 A LYS 636 A TYR 670 A MET 682 A GLN 683 A PHE 684 A ILE 685 A SER 687 A PRO 689 A HIS 745 A ASP 747 A ASN 748 A LEU 750 A PHE 758 A ILE 760 A ASP 761
	betulinic acid	64971	8.8540	323542.9688	A PHE 612 A LYS 613 A SER 614 A LEU 616 A PRO 618 A ILE 634 A LYS 636 A TYR 670 A MET 682 A PHE 684 A PRO 689 A GLU 692 A ASP 747 A ASN 748 A LEU 750 A PHE 758 A ILE 760 A ASP 761

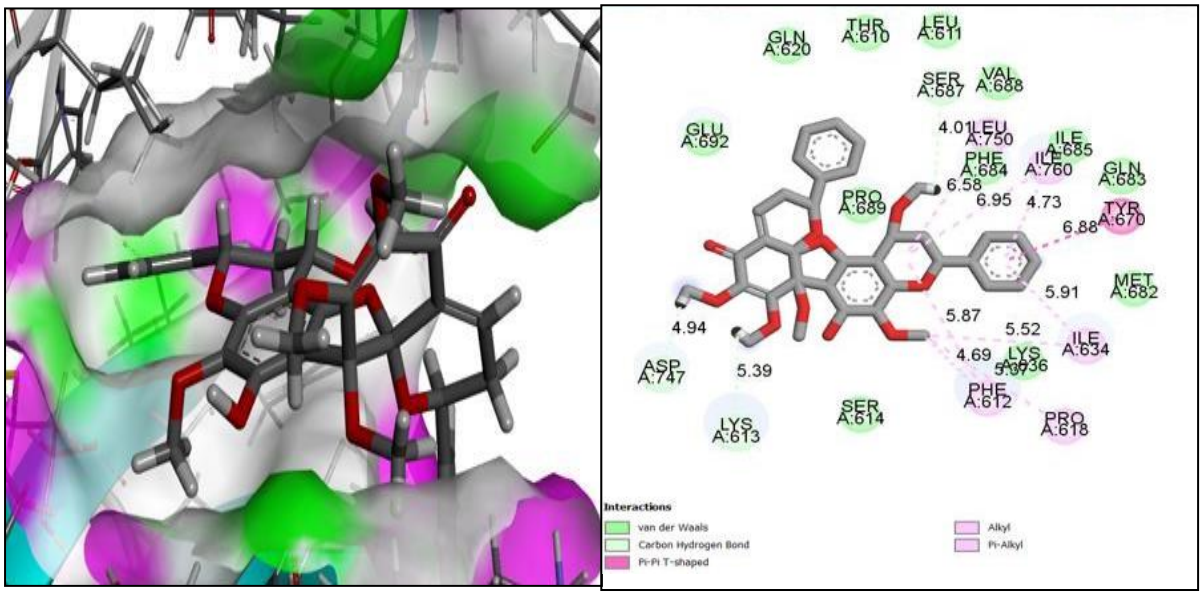

Figure 3: 3D & 2D interaction of 4UWH Protein with Calycopterone

Figure 3 depicts both 2D and 3D representations of the ligand Calycopterone interacting with the receptor, showcasing a binding energy of 9.5270 kcal/mol. The illustration presents the 4UWH protein divided into segments, with Calycopterone exhibiting diverse interactions in both 2D and 3D formats at specified distance. Notably, the active chemical, Calycopterone establishes carbon-hydrogen bonds with ASP-747, LYS-613 and SER-687 at distances of 4.94 Å, 5.39 Å and 4.01 Å, respectively. Additionally, In table 2 van der Waals interactions occur with residues GLU-692, THR-610, LEU-611, VAL-688, PRO-689, PHE-684, ILE-685, GLN-683, MET-682, LYS-636, SER-614, while alkyl bonds form with residues PHE-612, PRO-618, ILE-634, ILE-760, and LEU-750, with distances ranging from 5.87 Å to 6.58 Å.

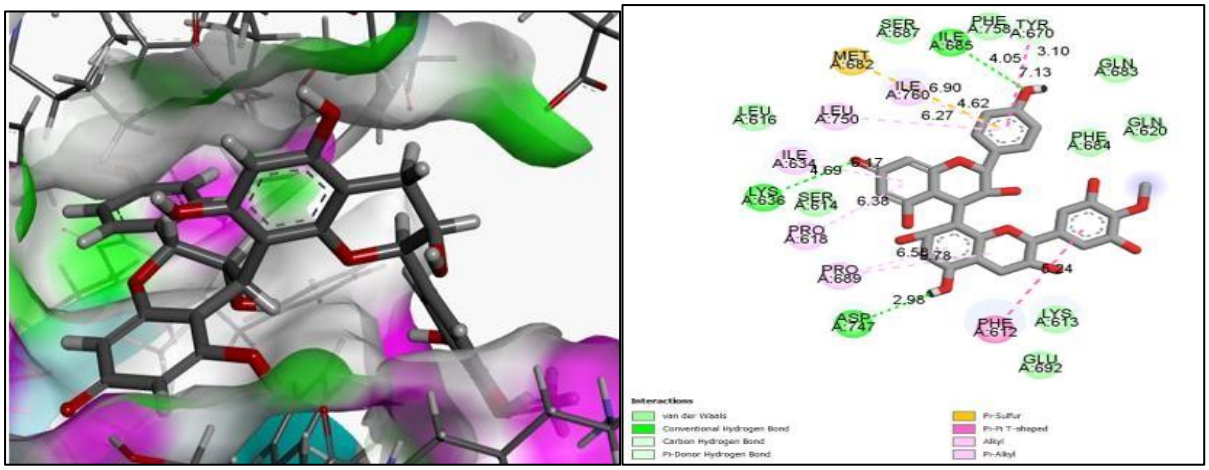

Figure 4: 3D & 2D interaction of 4UWH Protein with Proanthocyanidin

Figure 4 shows 3D and 2D representations of the ligand Proanthocyanidin with receptor with binding energy 9.4920 kcal/mol. The figure shows divided results of 4uwh protein and Proanthocyanidin in 3D and 2D formats with varied interactions at given distances. Proanthocyanidin, the active chemical, formed carbon-hydrogen bond interactions with TYR-670, residues. LYS-636, ASP-747, and ILE-685 have hydrogen bond interactions at distances of 6.17 Å, 2.98 Å, and 4.05 Å, respectively. At a distance of 4.62 Å, van der Waals interactions with SER-687, LEU-616, SER-614, GLU-692, LYS-613, PHE-684, GLN-620, GLN-683, PHE-758, and pi-sulfur interactions with MET-682. pi-pi T-shaped interactions with PHE-612 residues at a distance of 5.24 Å. Alkyl interactions with ILE-760, LEU-750, ILE-634, PRO-618, and PRO-689 at 6.90 Å, 6.27 Å, 4.69 Å, 6.38 Å, and 6.58 Å, respectively.

Table 3: Top 5 Docking results of the protein JAK(5LWM) docked with selected ligands.

Target protein	Compoundname	Compound id	Bind.energy [kcal/ mol]	Dissoc. constant [pM]	Contacting receptor residues
5LWM	Rutin	5280805	10.112 0	38708 .4453	A LEU 828 A GLY 829 A LYS 830 A GLY 831 A ASN 832 A PHE 833 A GLY 834 A SER 835 A VAL 836 A LYS 855 A GLU 871 A VAL 884 A MET 902 A TYR 904 A LEU 905 A GLY 908 A CYS 909 A ARG 953 A ASN 954 A LEU 956 A ALA 966 A ASP 967 A PHE 968 A GLY 969 A LEU 970
	Nicotiflorin	5318767	9.8700	58236 .3398	A LEU 828 A GLY 829 A LYS 830 A GLY 831 A ASN 832 A PHE 833 A GLY 834 A SER 835 A VAL 836 A LYS 855 A GLU 871 A VAL 884 A LEU 900 A MET 902 A TYR 904 A LEU 905 A GLY 908

					A CYS 909 A ARG 953 A ASN 954 A LEU 956 A ALA 966 A ASP 967 A PHE 968 A GLY 969 A LEU 970
	1,3,6-tri-O-galloyl-beta-D-glucose	452707	9.7350	73139.2266	A LEU 828 A GLY 829 A LYS 830 A GLY 831 A PHE 833 A GLY 834 A SER 835 A VAL 836 A ALA 853 A LYS 855 A LEU 857 A GLN 864 A VAL 884 A MET 902 A GLU 903 A TYR 904 A LEU 905 A GLY 908 A CYS 909 A ARG 911 A ASP 912 A ARG 953 A ASN 954 A LEU 956 A ALA 966 A ASP 967 A GLY 969 A LEU 970
	Vitexin	5280441	9.6740	81070.7109	A LEU 828 A GLY 829 A LYS 830 A GLY 831 A SER 835 A VAL 836 A ALA 853 A LYS 855 A VAL 884 A MET 902 A GLU 903 A TYR 904 A LEU 905 A GLY 908 A CYS 909 A ASP 912 A ARG 953 A ASN 954 A LEU 956 A ALA 966 A ASP 967
	3'-O-Methyl ellagic acid 4-xyloside	101949535	9.5860	94052.1719	A GLN 827 A LEU 828 A GLY 829 A VAL 836 A ALA 853 A LYS 855 A VAL 884 A MET 902 A GLU 903 A TYR 904 A LEU 905 A PRO 906 A SER 907 A GLY 908 A CYS 909 A ARG 953 A LEU 956 A ALA 966 A ASP 967

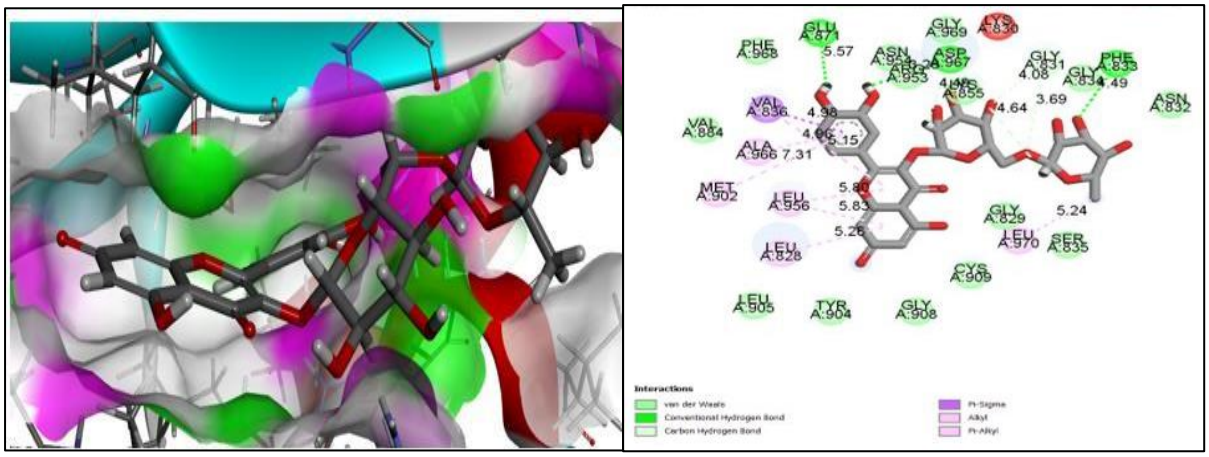

Figure 5:3D & 2D interaction of 5LWM Protein with Rutin

Figure 5 shows 2D and 3D representations of the ligand Rutin with receptor with binding energy 10.1120 kcal/mol. The figure shows divided results of 5lwm protein and Rutin in 3D and 2D formats with varied interactions at given distances. Rutin, the active molecule, formed hydrogen bonds with residues GLU-871, ASP-967, and PHE-833 at distances of 5.57 Å, 3.26 Å, and 4.49 Å, respectively. In table 3 van der Waals interactions with PHE-968, VAL-884, LEU-905, TYR-904, GLY-908, CYS-909, GLY-829, SER-835, ASN-832, GLY-834, GLY-969, ASN-954, ARG-953 and alkyl bonds with ALA-966, MET-902, LEU-956, LEU-828, LEU-970 at 4.96 Å, 7.31 Å, 5.80 Å, 5.26 Å, 5.24 Å and pi-sigma bonds with residues VAL-836 at the distances of 4.98 Å respectively.

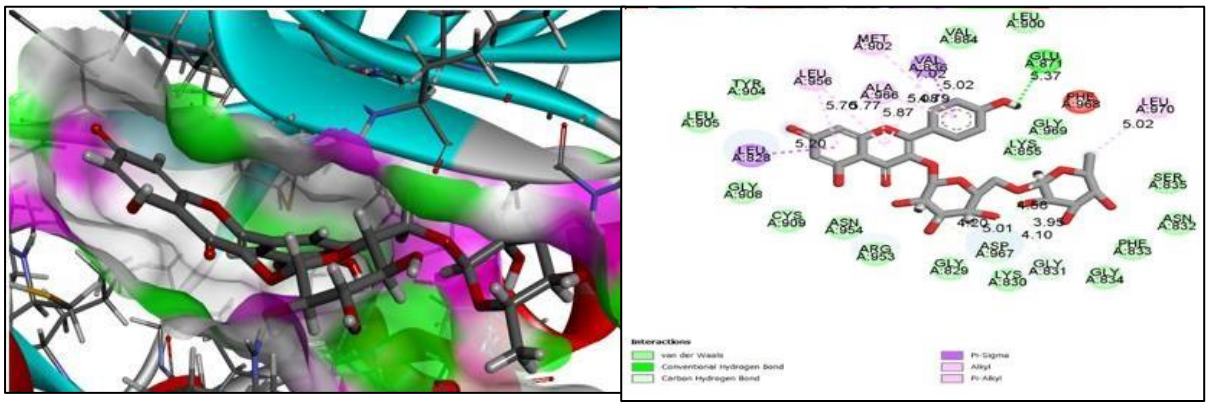

Figure 6: 3D & 2D interaction of 5LWM Protein with Nicotiflorin

Figure 6 shows 2D and 3D representations of the ligand Nicotiflorin with receptor with binding energy 9.8700 kcal/mol. The figure 6 shows divided results of 5lwm protein and Nicotiflorin in 3D and 2D formats with varied interactions at given distances. Nicotiflorin, the active chemical, formed hydrogen bond interactions with residues GLU-871 at distances of 5.37 Å. Interactions of van der Waals forces with residues TYR-904, LEU-905, GLY-908, CYS-909, ASN-954, ARG-953, GLY-829, LYS-830, GLY-834, PHE-833, ASN-832, SER-835, LYS-855, GLY-969, VAL-884, LEU-900, and pi-sigma interactions with residues VAL-836, LEU-828 at 5.02 Å, 5.20 Å distances. Alkyl interactions with residues LEU-956, ALA-966, MET-902, and LEU-970 at 5.76 Å, 5.87 Å, 7.02 Å, and 5.02 Å, respectively shown in Table 4.

Table 4: Top 5 Docking results of the protein BRAF(6P3D) docked with selected ligands.

Target protein	Compound name	Compound id	Bind. energy [kcal/mol]	Diss oc. con stan t [pM]	Contacting receptor residues
	beta-carotene	5280489	10.6220	1636 7.06 35	A ILE 463 A PHE 468 A VAL 471 A ALA 481 A VAL 482 A LYS 483 A ASN 500 A GLU 501 A

					VAL 504 A LEU 505 A LEU 514 A ILE 527 A THR529 A GLN 530 A TRP 531A CYS 532 A SER 571 A ILE 572 A ILE 573 A HIS 574 A ARG 575 A PHE 583A GLY 593 A ASP 594 A PHE 595 A LEU 597
6P3D	Trigallic Acid	90470472	10.3380	2643 2.94 34	A ILE 463 A VAL 471 A ALA 481 A VAL 482 A LYS 483 A GLU 501 A VAL 504 A LEU 505 A THR 508 A ILE 513 A LEU514 A ILE 527 A THR 529 A TRP 531 A CYS 532 A LEU 567 A HIS 574 A PHE583 A ILE 592 A GLY 593 A ASP 594 A PHE 595 A LEU 597
	Taraxerol	92097	9.8310	6219 8.71 88	A PHE 468 A ALA 497 A ASN 500 A GLU 501 A VAL 504 A LEU 505 A THR 508 A ILE 513 A LEU567 A ILE 572 A ILE 573 AHIS 574 A ARG 575 A ASP576 A GLY 593 A ASP 594
	Cosmosiin	5280704	9.7510	7119 0.53 13	A ILE 463 A VAL 471 A ALA 481 A VAL 482 A LYS 483 A GLU 501 A LEU505 A LEU 514 A ILE 527 A THR 529 A GLN 530 A TRP 531 A CYS 532 A GLY534 A SER 535 A SER 536 A HIS 539 A ASN 580 A PHE 583 A ASP 594 A PHE595 A LEU 597
	Friedelin	91472	9.7190	7514 1.27 34	A ASN 500 A GLU 501 A VAL 504 A LEU 505 A THR 508 A ILE 513 A LEU567 A ILE 572 A ILE 573 AHIS 574 A ARG 575 A GLY593 A ASP 594

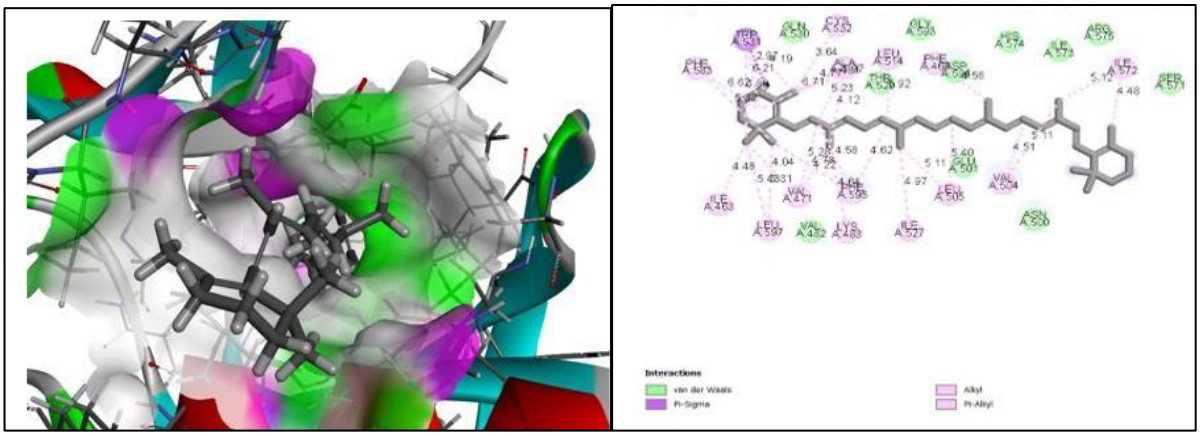

Figure 7: 3D & 2D interaction of 6P3D Protein with beta-carotene

Figure 7 shows 2D and 3D representations of the ligand beta-carotene with receptor with binding energy 10.6220 kcal/mol. Docked findings of 6p3d protein and beta-carotene in 3D and 2D formats with varied interactions at set distances are shown in the figure. At 6.21 Å distances, the active chemical, beta-carotene, displayed van der Waals contacts with residues

GLN-530, GLY-593, THR-529, ASP-594, HIS-574, ILE-573, ARG-575, SER-571, ASN-500, GLU-501, VAL-482, and pi-sigma interactions with residues TRP-531. PHE-583, CYC-532, ALA-589, LEU-514, PHE-469, ILE-572, VAL-504, LEU-505, ILE-527, PHE-595, LYS-483, VAL-471, LEU-597, ILE-463 at distances of 5.82 Å, 3.64 Å, 6.71 Å, 4.77 Å, 4.56 Å, 5.12 Å, 4.51 Å, 5.40 Å, 4.97 Å, 4.62 Å, 4.22 Å, 5.28 Å, 4.04 Å, and 4.48 Å in table 4.

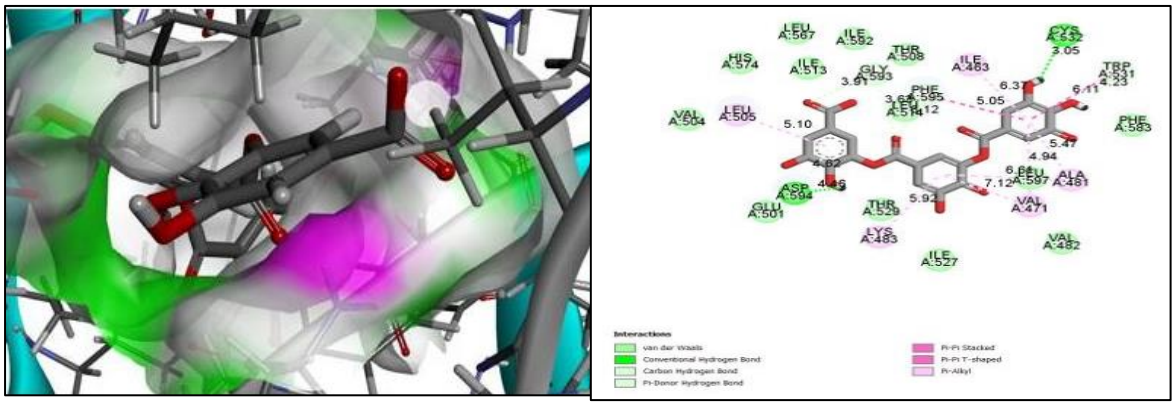

Figure 8: 3D & 2D interaction of 6P3D Protein with Trigallic Acid

Figure 8 shows 2D and 3D representations of the ligand Trigallic Acid with receptor with binding energy 10.3380 kcal/mol. The figure depicts docking results of the 6p3d protein and Trigallic Acid in 3D and 2D formats with various interactions at given distances. Trigallic Acid, the active chemical, formed hydrogen bond interactions with ASP-594 and CYS-532 at distances of 4.46 Å and 3.05 Å, respectively. THR-508, LEU-514, PHE-583, LEU-597, VAL-482, ILE-527, THR-529, GLU-501, and carbon-hydrogen bond interactions with residues TRP-531, GLY-593 at distances of 4.23 Å, 3.91 Å. pi-alkyl interactions with LEU-505, ILE-463, ALA-481, VAL-471, and LYS-483 at distances of 5.10 Å, 6.37 Å, 5.47 Å, 4.94 Å, and 5.92 Å.

Molecular Dynamics Simulation

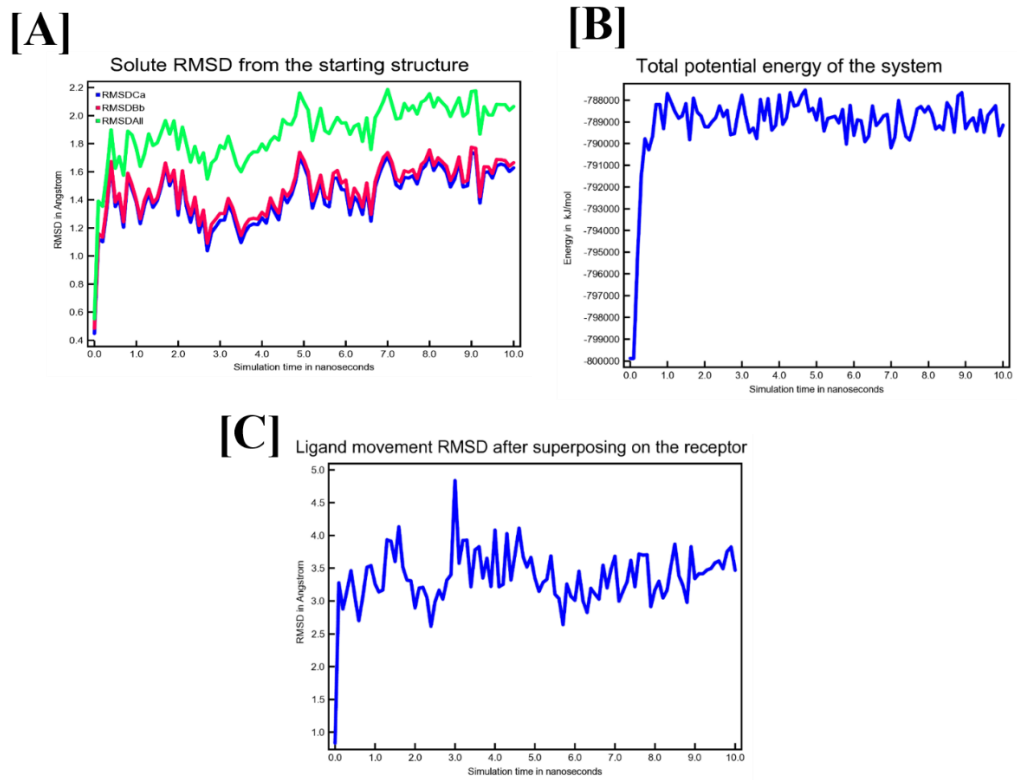

Figure 9: [A]The molecular motions of BRAF: beta-carotene in RMSD [Å] (with respect to starting structure – red colour) (blue color-carbon α atoms, magenta colour-backbone and green colour-all components) as a function of time. [B] The molecular motions of the BRAF:

beta-carotene in energy (blue colour) [kcal/mol] as a function of time. [C] Ligand movement RMSD after superposing on the receptor (BRAF)

Figure 9 A depicts the plot of' solute RMSD from the initial structure' vs simulation time. The above plot shows that the complex fluctuated between 0.0 and 7.0 ns, after which it remained rather stable and equilibrium was attained. From 7 to 10 ns, the protein-ligand combination remains stable. The RMSD variations were found to be limited to a range of 1.2-2.0 Å. The figure clearly indicates that the ligand binds to the protein and keeps it stable.

The above plot indicates that the total potential energy of the system fluctuated within an acceptable range of -791000 kJ/mol to -788000 kJ/mol during the simulation, supporting the correctness of the simulation presented in Fig. 9B. The above plot shows that the RMSD of the ligand heavy atoms ranged largely between 1.0 Å and 3.5 Å, occasionally exceeding 3.5 Å, indicating a small imbalance in interaction in Fig. 9C.

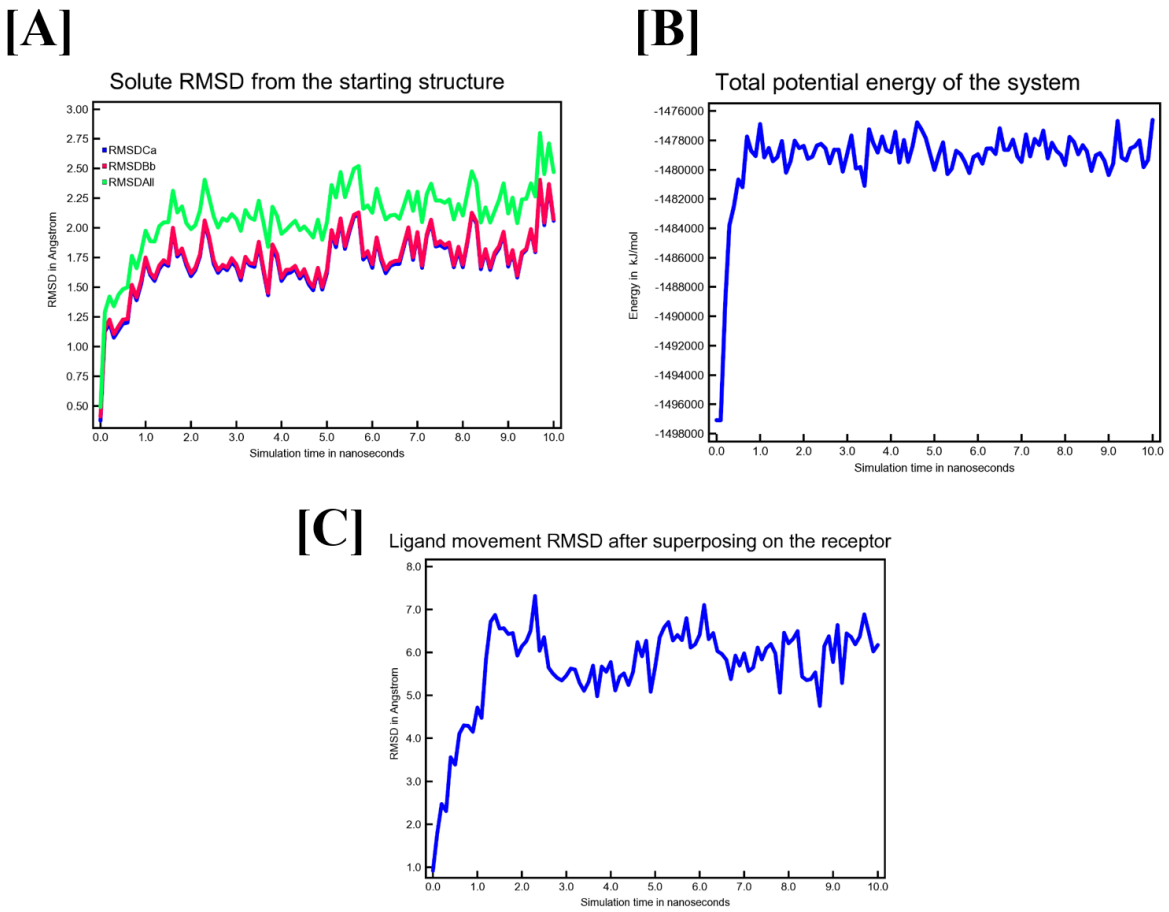

Figure 10: [A]The molecular motions of PI3K: Calycopterone in RMSD [Å] (with respect to starting structure – red colour) (blue colour-carbon α atoms, magenta colour-backbone and green colour-all components) as a function of time. [B] The molecular motions of the PI3K: Calycopterone in energy (blue colour) [kcal/mol] as a function of time [C] Ligand movement RMSD after superposing on the receptor (PI3K)

Figure 10 A depicts the plot of' solute RMSD from the initial structure' vs simulation time. The above plot shows that the complex fluctuated between 0.0 and 5.0 ns, after which it remained rather steady and equilibrium was attained. From 5 to 10 ns, the protein-ligand combination remains stable. The RMSD variations were found to be limited to a range of 1.00-2.25 Å. The figure clearly indicates that the ligand binds to the protein and keeps it stable. It can be inferred from the above plot that during the simulation's progress, the system's total potential energy fluctuated within an acceptable range of −1482000 kJ/mol to −1478000 kJ/mol, therefore indicating the validity of the simulation in Fig 10B. It can be inferred from the above plot that RMSD of the ligand heavy atoms fluctuated mostly between a stable 1.0 Å to 6.0 Å, occasionally going over 6.0 Å indicating slight imbalance in interaction showing in Fig 10C.

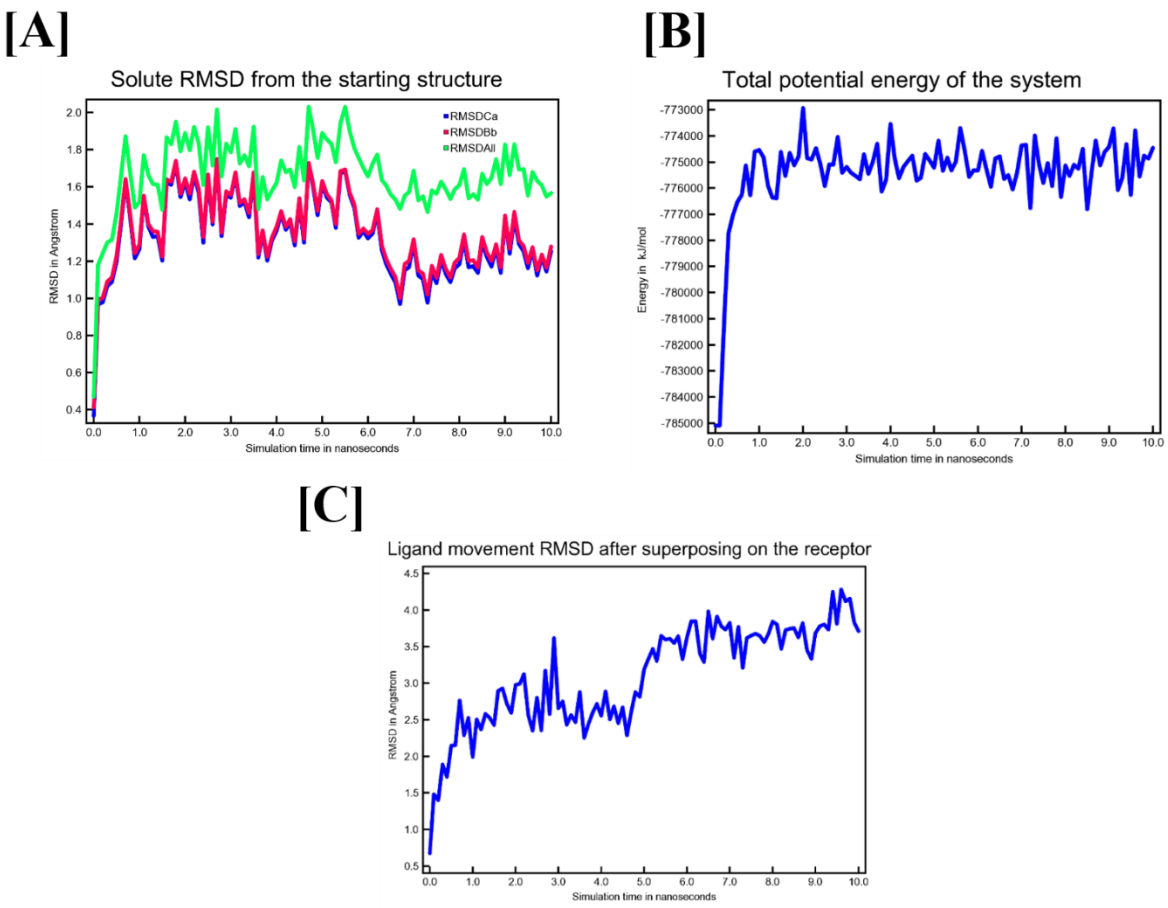

Figure 11: [A]The molecular motions of JAK: Rutin in RMSD [Å] (with respect to starting structure – red colour) (blue colour-carbon α atoms, magenta colour-backbone and green colour-all components) as a function of time. [B] The molecular motions of the JAK: Rutin in energy (blue colour) [kcal/mol] as a function of time [C] Ligand movement RMSD after superposing on the receptor (JAK)

Fig. 11A shows 'solute RMSD from the starting structure' plotted against the simulation time. It can be inferred from the above plot that around 0.0 to 7.0 ns is fluctuated, thereafter, the complex remained reasonably stable, and equilibrium was achieved. The protein-ligand complex maintains stability from 7 to 10 ns. RMSD fluctuations were found to be confined within a range of 1.00- 1.8Å. Fig clearly shows that the ligand binds with the protein and maintains stability.

The above plot indicates that the system's total potential energy fluctuated within an acceptable range of -777000 kJ/mol to -774000 kJ/mol over the simulation's progress, verifying the simulation's validity in Fig 11B. Fig 11C shows the plot indicates that the RMSD of the ligand-heavy atoms ranged largely between 1.0 Å and 3.5 Å, occasionally exceeding 3.5 Å, indicating a small imbalance in interaction.

DISCUSSION

Cancer fatalities are a serious problem all over the world. The Combretaceae family contains a lot of flavonoids and has antimutagenic and anticancer effects. These 16 Combretaceae plants were gathered in order to fight cancer. *Anogeissus acuminata, Combretum quadrangulare, Terminalia chebula, Terminalia bellarica, Terminalia catappa L., Anogeissus latifolia, Combretum imberbe, Guiera senegalensis, Combretum albidum, Combretum indicum, Terminalia pallida, Terminalia ivorensis, Lumnitzera racemose, Conocarpus erectus, Getonia floribunda, Terminalia alata,* are a member of the combretaceae family.

The PI3K pathway has emerged as an important target for cancer treatment. In some malignancies, the PI3K-Akt signalling pathway is abnormally active (Fumarola *et al.*, 2014). The majority of oncoproteins and tumour suppressors are involved in cell metabolic/signaling regulation, which converges among the PI3K signal transduction pathway in an equilibrium

altered in different human malignancies by activating and inactivating processes, targeting these inter-related proteins. Deregulation of the PI3K communication pathway may be a critical event in the cancer process due to the prevalence of oncogenic activating mutations and genetic inactivation of tumour suppressors that regulate the system (Altomare and Testa, 2005). Somatic PIK3CA mutations are seen in up to 30% of common epithelial malignancies, including breast, colon, prostate, and mucous membrane tumours (Patel *et al.*, 2021).

Janus kinases (JAK) are involved in both normal and malignant cell proliferation, differentiation, and apoptosis. JAK1, JAK3, and TYK2 mutations have been found in acute adult leukaemias as well as prevalent solid malignancies (breast, colorectal, lung, gastric, and hepatocellular carcinomas (Jeong *et al.*, 2008). Janus kinase 3 (JAK3) is an intriguing therapeutic target for the treatment of inflammatory illnesses, autoimmune disorders, organ transplant rejection, and cancer (Balupuri, Balasubramanian and Cho, 2020). JAK3 activating mutations have been identified in a variety of leukaemias and lymphomas, including NKTL, monomorphic epitheliotropic intestinal T-cell lymphoma, T-cell acute lymphoblastic leukaemia, and hepatosplenic T-cell lymphoma. The abnormal activation of JAK3 in haematological malignancies suggests that JAK3 could be a therapeutic target for cancer (Nairismägi *et al.*, 2018). ARAF (also known as A-Raf), BRAF (B-Raf), and CRAF (c-Raf or Raf-1) are three highly conserved RAF genes, and knockout experiments in mice show that their protein products perform diverse functions (Surveillance Epidemiology, 2019). A glutamic acid for valine substitution at position 600 (V600E) is the most frequent BRAF mutation, accounting for more than 90% of cancer cases involving this gene (Hou, Liu and Xing, 2007). BRAFV600E is activated roughly 500-fold, and it triggers constitutive ERK signalling via hyperactivation of the RAS-MEK-ERK pathway, as well as constitutive nuclear factor kappa-B (NF-B) signalling in response, boosting proliferation, survival, and transformation (Lin *et al.*, 2010).

Because of the ubiquity of abnormal PI3K signalling in human cancer cells, PI3K has become an intriguing target for the development of anticancer medicines [29]. JAK/STAT3 signalling activity is abnormal in a wide range of human tumours, including haematological malignancies and solid tumours such as head and neck, breast, and prostate cancers [30]. The RAF protein kinase family includes B-RAF, which is one of the enzymes involved in the growth of many malignancies. The therapeutic target of the V600E-BRAF protein has considerable scientific promise (Bartholomeusz and Gonzalez-Angulo, 2012).

CONCLUSION

The protein-ligand interaction plays a significant role in structural-based drug discovery/designing. In the present work, we have taken the receptors (PI3K, JAK, BRAF) and analyzed 196 natural compounds library shortlisted from published literature with proven anticancer activity. The family Combretaceae has demonstrated pharmacological benefits such as anti-leishmanial, cytotoxic, antibacterial, antidiabetic, antitoxin, antitumor, and antifungal. After molecular docking with (4UWH), (5LWM), and (6P3D) based on docking score Calycopterone, Rutin, and beta-carotene was identified as the best compound. Rutin is a rutinoside, which is quercetin with a sugar group substitution at position C-3 for the hydroxyl group. It functions as an antioxidant and metabolite. Beta-carotene is a natural retinol (vitamin A) precursor obtained from certain fruits and vegetables with anticancer and chemopreventive activity. As an antioxidant, beta-carotene inhibits free radicals that damage DNA. Based on the findings it can be concluded that further studies, including *In vitro* and *in vivo* experiments, are needed to confirm the efficacy of these compounds.

ACKNOWLEDGMENT

We acknowledge GUJCOST, DST, Government of Gujarat, for providing the Super-computing facility, and GSBTM, DST, Government of Gujarat, for providing the BIN-Node Facility to the department. Author Poojaben Prajapati would like to thank Dr. Saumya K. Patel for providing the facility. Author Poojaben Prajapati would like to acknowledge the ScHeme of Developing High-quality Research (SHODH), Education Department, Government of Gujarat, INDIA, for providing the student support fellowship.

AUTHORS' CONTRIBUTIONS

Pooja Prajapati: Software, Methodology, Data Analysis, Writing – original manuscript, Writing – review & editing. **Rakesh M. Rawal**: Visualization, Supervision, Investigation. **Bharat Maitreya**: Visualization, Supervision, Writing – review & editing.

CONFLICT OF INTEREST

All the authors have no conflict of interest.

REFERENCES

1. Ai, D. *et al.* (2021) 'TRPS1: a highly sensitive and specific marker for breast carcinoma, especially for triple-negative breast cancer', *Modern Pathology*, 34(4), pp. 710–719. doi: 10.1038/s41379-020-00692-8.
2. Allouche, A. (2012) 'Software News and Updates Gabedit — A Graphical User Interface for Computational Chemistry Softwares', *Journal of computational chemistry*, 32, pp. 174–182. doi: 10.1002/jcc.
3. Altomare, D. A. and Testa, J. R. (2005) 'Perturbations of the AKT signaling pathway in human cancer', *Oncogene*, 24(50), pp. 7455–7464. doi: 10.1038/sj.onc.1209085.
4. Anderson, K. E. *et al.* (2021) 'Reports of Forgone Medical Care among US Adults during the Initial Phase of the COVID-19 Pandemic', *JAMA Network Open*, 4(1), pp. 1–11. doi: 10.1001/jamanetworkopen.2020.34882.
5. Balupuri, A., Balasubramanian, P. K. and Cho, S. J. (2020) '3D-QSAR, docking, molecular dynamics simulation and free energy calculation studies of some pyrimidine derivatives as novel JAK3 inhibitors', *Arabian Journal of Chemistry*, 13(1), pp. 1052–1078. doi: 10.1016/j.arabjc.2017.09.009.
6. Bartholomeusz, C. and Gonzalez-Angulo, A. M. (2012) 'Targeting the PI3K signaling pathway in cancer therapy', *Expert Opinion on Therapeutic Targets*, 16(1), pp. 121–130. doi: 10.1517/14728222.2011.644788.
7. Corcoran, R. B. *et al.* (2015) 'Combined BRAF and MEK inhibition with dabrafenib and trametinib in BRAF V600-Mutant colorectal cancer', *Journal of Clinical Oncology*, 33(34), pp. 4023–4031. doi: 10.1200/JCO.2015.63.2471.
8. Courtney, K. D., Corcoran, R. B. and Engelman, J. A. (2010) 'The PI3K pathway as drug target in human cancer', *Journal of Clinical Oncology*, 28(6), pp. 1075–1083. doi: 10.1200/JCO.2009.25.3641.
9. Eloff, J. N., Katerere, D. R. and McGaw, L. J. (2008) 'The biological activity and chemistry of the southern African Combretaceae', *Journal of Ethnopharmacology*, 119(3), pp. 686–699. doi: 10.1016/j.jep.2008.07.051.
10. Factor, I. (2022) 'Herbal Plants: A Study of Phytochemicals', (111), pp. 111–114.
11. Fanelli, G. N. *et al.* (2020) 'The heterogeneous clinical and pathological landscapes of metastatic Braf-mutated colorectal cancer', *Cancer Cell International*, 20(1), pp. 1–12. doi: 10.1186/s12935-020-1117-2.
12. Fumarola, C. *et al.* (2014) 'Targeting PI3K/AKT/mTOR pathway in non small cell lung cancer', *Biochemical Pharmacology*, 90(3), pp. 197–207. doi: 10.1016/j.bcp.2014.05.011.
13. Ghoshal, S. *et al.* (2022) 'Institutional Surgical Response and Associated Volume Trends Throughout the COVID-19 Pandemic and Postvaccination Recovery Period', *JAMA Network Open*, 5(8), p. E2227443. doi: 10.1001/jamanetworkopen.2022.27443.
14. Hanahan, D. (2022) 'Hallmarks of Cancer: New Dimensions', *Cancer Discovery*, 12(1), pp. 31–46. doi: 10.1158/2159-8290.CD-21-1059.
15. Hong, D. S. *et al.* (2012) 'BRAF(V600) inhibitor GSK2118436 targeted inhibition of mutant BRAF in cancer patients does not impair overall immune competency', *Clinical Cancer Research*, 18(8), pp. 2326–2335. doi: 10.1158/1078-0432.CCR-11-2515.
16. Hou, P., Liu, D. and Xing, M. M. (2007) 'Functional characterization of the T1799-1801del and A1799-1816ins BRAF mutations in papillary thyroid cancer', *Cell Cycle*, 6(3), pp. 377–379. doi: 10.4161/cc.6.3.3818.
17. Hu, X. *et al.* (2021) 'The JAK/STAT signaling pathway: from bench to clinic', *Signal Transduction and Targeted Therapy*, 6(1). doi: 10.1038/s41392-021-00791-1.
18. Jeong, E. G. *et al.* (2008) 'Somatic mutations of JAK1 and JAK3 in acute leukemias and solid cancers', *Clinical Cancer Research*, 14(12), pp. 3716–3721. doi: 10.1158/1078-0432.CCR-07-4839.

19. Keute, M. *et al.* (2019) 'No modulation of pupil size and event-related pupil response by transcutaneous auricular vagus nerve stimulation (taVNS)', *Scientific Reports*, 9(1), pp. 1–10. doi: 10.1038/s41598-019-47961-4.
20. Kim, B. H. *et al.* (2020) 'STAT3 Inhibitor ODZ10117 Suppresses Glioblastoma Malignancy and Prolongs Survival in a Glioblastoma Xenograft Model', *Cells*, 9(3), pp. 1–16. doi: 10.3390/cells9030722.
21. Krieger, E. and Vriend, G. (2015) 'New ways to boost molecular dynamics simulations', *Journal of Computational Chemistry*, 36(13), pp. 996–1007. doi: 10.1002/jcc.23899.
22. Lin, K. *et al.* (2010) 'The role of B-RAF mutations in melanoma and the induction of EMT via dysregulation of the NF-κB/snail/RKIP/PTEN circuit', *Genes and Cancer*, 1(5), pp. 409–420. doi: 10.1177/1947601910373795.
23. Liu, K., Watanabe, E. and Kokubo, H. (2017) 'Exploring the stability of ligand binding modes to proteins by molecular dynamics simulations', *Journal of Computer-Aided Molecular Design*, 31(2), pp. 201–211. doi: 10.1007/s10822-016-0005-2.
24. Massarotti, A. *et al.* (2012) 'The tubulin colchicine domain: A molecular modeling perspective', *ChemMedChem*, 7(1), pp. 33–42. doi: 10.1002/cmdc.201100361.
25. Nairismägi, M. L. *et al.* (2018) 'Oncogenic activation of JAK3-STAT signaling confers clinical sensitivity to PRN371, a novel selective and potent JAK3 inhibitor, in natural killer/T-cell lymphoma', *Leukemia*, 32(5), pp. 1147–1156. doi: 10.1038/s41375-017-0004-x.
26. Patel, C. N. *et al.* (2021) 'Pinpointing the potential hits for hindering interaction of SARS-CoV-2 S-protein with ACE2 from the pool of antiviral phytochemicals utilizing molecular docking and molecular dynamics (MD) simulations', *Journal of Molecular Graphics and Modelling*, 105(February 2020), p. 107874. doi: 10.1016/j.jmgm.2021.107874.
27. Pinzi, L. and Rastelli, G. (2019) 'Metode berbasis struktur bergantung pada informasi yang diperoleh dari pengetahuan tentang struktur 3D target yang menarik, dan mereka memungkinkan database peringkat molekul sesuai dengan struktur dan komplementaritas elektronik ligan ke target tertentu', *igms in drug discovery. InternatInPinzi, L., & Rastelli, G. (2019). Molecular docking: Shifting paradional Journal of Molecular Sciences, 20(18). https://doi.org/10.3390/ijms20184331ternational Journal of Molecular Sciences*, 20(18), pp. 1–23.
28. Prajapati, P. *et al.* (2023) 'Computational Analysis of Transcription Factors As Cancer Drug Targets With Potential Inhibitors From the Npact Database', *International Association of Biologicals and Computational Digest*, 2(2), pp. 14–26. doi: 10.56588/iabcd.v2i2.97.
29. Surveillance Epidemiology (2019) 'Colorectal Cancer - Cancer Stat Facts', *SEER Cancer Stat Facts: Colorectal Cancer*, 9(1), p. 2. Available at: https://seer.cancer.gov/statfacts/html/colorect.html.
30. Trayes, K. P. and Cokenakes, S. E. . (2021) 'Treatment Cancer Breast', *Am Fam Physician*, 104(2), pp. 171–178.
31. Velavan, S. (2016) 'Phytochemical Techniques - A Review', *World Journal of Science and Research*, 1(3), pp. 80–91.
32. Wong, K. K., Engelman, J. A. and Cantley, L. C. (2010) 'Targeting the PI3K signaling pathway in cancer', *Current Opinion in Genetics and Development*, 20(1), pp. 87–90. doi: 10.1016/j.gde.2009.11.002.